Parameter Estimation for Low-Mass Eccentric Black Hole Binaries

Katelyn J. Wagner and R. O'Shaughnessy
Center for Computational Relativity and Gravitation, Rochester Institute of Technology, Rochester, New York 14623, USA

Recent studies have shown that orbital eccentricity may indicate dynamical assembly as a formation mechanism for binary black holes. Eccentricity leaves a distinct signature in gravitational wave signals and it may be measured if the binary remains eccentric when it enters the LIGO band. Although eccentricity has not yet been confidently detected, the possibility of detecting eccentric binaries is becoming more likely with the improved sensitivity of gravitational wave detectors such as LIGO, Virgo, and KAGRA. It is crucial to assess the accuracy of current search pipelines in recovering eccentricity from gravitational wave signals if it is present. In this study, we investigate the ability of parameter estimation pipeline RIFT to recover eccentricity in the non-spinning and aligned-spin cases for low mass binary black holes. We use `TaylorF2Ecc` and `TEOBResumS` to inject sets of synthetic signals and test how well RIFT accurately recovers key binary black hole parameters. Our findings provide valuable insights into the capability of current parameter estimation methods to detect and measure eccentricity in gravitational wave signals.

I. INTRODUCTION

Advanced LIGO [1] and Virgo [2] ground-based gravitational wave (GW) detectors have now discovered more than 90 compact binary mergers, including a few neutron star-black hole mergers and binary neutron star mergers [3]. Most isolated compact binaries that enter the LIGO band at 10Hz are expected to display quasi-circular orbits due to gravitational radiation decaying their orbits over time [4]. However, recent studies have suggested that some binary black hole systems may instead display eccentric orbits before merging [5–7]. These eccentric binaries are expected to be short-lived, but they offer a unique opportunity to probe the formation channels of binary black holes.

Viable formation channels for binary black holes fall broadly into two categories: isolated binary evolution and dynamical assembly. The intrinsic parameters of a binary, including component masses, component spins, and eccentricity, can provide information about its history. Gravitational waves can be used to probe these parameters.

The most likely formation channel for binary black holes is thought to be through the evolution of massive binary stars—but eccentric orbits are not expected to result from this channel [8]. One proposed mechanism for forming eccentric binary black holes involves the dynamical interactions of single black holes in densely populated stellar environments [9], such as globular clusters, nuclear star clusters, or galactic centers [10–13]. In these environments, the progenitors do not encounter each other until they have already evolved into black holes. Then, the dynamical assembly of binaries occurs as a series of gravitational interactions with other black holes. Interactions in such environments are frequent, and objects may enter and leave any number of binaries before eventually merging. The orbit is hardened in each successive interaction and may merge while eccentricity is still present [10].

Understanding the formation channels of binary black holes is crucial for interpreting gravitational wave observations and constraining theoretical models, as different formation mechanisms leave signatures in gravitational wave signals. The presence of eccentricity in a signal may be an excellent probe for the dynamical formation channel [14–16], and eccentric mergers may occur frequently enough that gravitational waves can be used to find them. However, detecting eccentricity in binary black hole systems is challenging due to the low expected signal-to-noise ratio (SNR) of eccentric gravitational wave detections. In addition, eccentric waveforms are more complicated waveforms than those of quasi-circular systems.

Eccentricity creates distinctive and observationally-accessible modulations in gravitational wave signals, making it key to understanding the formation and evolution of compact binaries. As the sensitivity of ground-based detectors has increased for the next observing run, a better understanding of our ability to recover eccentricity is vital. As for any GW detection, parameter estimation and model selection are key in performing an analysis [17], so an understanding of the performance of these tools is highly important.

Several studies have attempted to infer the eccentricity of binary black hole systems from the observed gravitational wave signals in O1 & O2 [18–23], in particular for GW190521 [24–26], as well as in O3 [27–32] . Many used parameter estimation and some currently available models that consider eccentric effects: `TEOBResumS` [33], and `SEOBNRE` [34]. Another model including eccentricity is `TaylorF2Ecc` [35]. Others have focused on high mass regimes

where the signal is much shorter so the analysis is more computationally efficient [31]. However, Favata *et al.* [14] show that low-mass systems enable much sharper constraints on eccentricity and the authors of [36] show that eccentricity is important for statements about population characteristics and source parameter recovery. In general, full parameter estimation may be limited in the low mass regime as signals are long and signal-to-noise ratio is lower, but the highly-parallelizable nature of RIFT [37, 38] makes it an excellent tool for this problem. Therefore, we can use RIFT to perform parameter estimation systematics for eccentric black hole binaries using multiple waveform models focusing on the low-mass regime to best constrain measurements of eccentricity.

The study of eccentric binary black holes remains an active area of research, and future detections by advanced gravitational wave detectors will provide new opportunities to study the dynamics and formation channels of these systems. In the meantime, we must quantitatively understand our ability to accurately recover eccentricity as we prepare for real detections.

In this paper, we perform a systematics study using RIFT [37, 38] to investigate how well eccentricity can be recovered for low-mass systems. Section II provides an overview of how RIFT performs parameter estimation. It also describes the waveform models used in this study and details the synthetic population created for this purpose. Section III discusses degeneracies between certain parameters relevant to this study, and includes confirmation of others' previous results using our methods. We describe the addition of a new parameter to our pipeline, mean periapsis anomaly, which was used in this context by [39]. Finally, the results of our systematics study are given in Section IV. We show recovery of eccentric non-spinning and aligned-spin injected signals for low-mass BBH using RIFT [37, 38].

II. METHODS

A. RIFT

A merging compact binary can be characterized by its intrinsic and extrinsic parameters. The intrinsic parameters, λ, refer to the component masses, component spins, eccentricity, and matter quantities. The seven extrinsic paramters (θ) describe the spacetime location and orientation of the system, including right ascension, declination, luminosity distance, coalescence time, inclination, orbital phase, and polarization.

RIFT is an iterative process consisting of two stages to estimate the intrinsic and extrinsic parameters of the binary source. It compares gravitational wave data to predicted signals $h_k(\boldsymbol{\lambda}, \boldsymbol{\theta})$ where k is the number of GW detectors. In the first stage, RIFT utilizes parallel computing to evaluate the marginal likelihood of each intrinsic parameter in a grid of candidate points via Monte Carlo

$$\mathcal{L}_{\rm marg}(\boldsymbol{\lambda}) = \int \mathcal{L}(\boldsymbol{\lambda}, \theta) p(\theta) d\theta.$$

This stage provides point estimates for $\ln \mathcal{L}_{\rm marg}(\boldsymbol{\lambda})$ using either Gaussian Process (GP) regression or random forests to interpolate a full posterior distribution over the intrinsic parameters.

In the second iterative stage, RIFT approximates $\mathcal{L}(\lambda)$ based on the set of evaluations $\{(\lambda_\alpha, \mathcal{L}_\alpha)\}$. The data is fitted for a full posterior distribution over the intrinsic parameters

$$p_{\rm post}(\boldsymbol{\lambda}) = \frac{\mathcal{L}_{\rm marg}(\boldsymbol{\lambda}) p(\boldsymbol{\lambda})}{\int d\boldsymbol{\lambda} \mathcal{L}_{\rm marg}(\boldsymbol{\lambda}) p(\boldsymbol{\lambda})}$$

where $p(\boldsymbol{\lambda})$ is the prior on the intrinsic parameters.

The posterior is fairly sampled to generate a new grid using adaptive Monte Carlo techniques. The grid is then fed back into the initial evaluation stage. After multiple iterations, the log-likelihood will converge to the true value for each parameter and the intrinsic samples will represent the true posterior distribution. Therefore, one learns the set of true parameters of the compact binary system.

Though RIFT is equipped to handle the non-spinning, aligned spin, and precessing spin cases, we do not explore precession in this study due to limited availability of waveforms that incorporate both eccentricity and precession.

In the course of this work, RIFT was extended to include the argument of periapsis, as this parameter is necessary to fully characterize generic eccentric orbits. The argument of periapsis is an angle that describes the initial orientation of a binary's orbital ellipse which affects the gravitational wave phase. Previous analyses using RIFT to infer the properties of black hole binaries using semi-analytic waveform models incorporating eccentricity have heretofore adopted a fixed value for the argument of peripasis [31]. More detail about mean periapsis anomoly is provided in Section III B.

B. Waveform Model

In this study, we use `TaylorF2Ecc` and `TEOBResumS` to characterize the gravitational radiation from black hole binaries in eccentric orbits. We use a given model both for generating synthetic

signals and in recovering their properties with parameter inference.

`TaylorF2Ecc` [35] is a quasi-Keplerian formalism describing post-Newtonian (PN) corrections to binary orbits, specifically in the low eccentricity regime. This formalism provides analytic solutions to the PN equations of motion, computing orbital quantities (r, ϕ) and their derivatives as a function of the eccentric anomoly [40, 41]. The quasi-Keplerian formalism enables one to track orbital evolution without computing ODEs. The `TaylorF2Ecc` waveforms are inspiral only. They extend the standard circular post-Newtonian approximations to incorporate eccentric effects for up to 3PN. The analytic solutions are given in [35]. Additionally, `TaylorF2Ecc` is an extension of the `TaylorF2` waveform, which is a frequency-domain approximant evaluated in the stationary-phase approximation and assumes circular orbits. In the $e_0 \to 0$ limit, where e_0 is the binary eccentricity at reference $f_0 = 10$Hz, the `TaylorF2Ecc` waveform reduces to `TaylorF2`. The value of f_0 is the low-frequency limit of the Advanced LIGO observing band. This waveform model is implemented in `lalsuite` [42].

`TEOBResumS` [43] is an effective-one-body (EOB) model. This approach combines the phases of two-body dynamics, including inspiral, merger, and ringdown, into a single analytical method. First introduced by [44], this method allows for highly accurate waveform calculations by mapping the dynamics of a binary system onto one single, effective object that moves in the potential. The effective object is described by equations of motion derived from general relativity. `TEOBResumS` is informed by NR simulations of BBH coalescence events for calibration and validation, particularly for the eccentric version of this model. Here, we use the eccentric spin-aligned waveforms from `TEOBResumS` [45] which were verified by NR for eccentricities up to $e \leq 0.3$ at 10 Hz. This model also incorporates higher order modes up to $l = |m| = 5$, except for $m = 0$. The user can also define the reference frequency for `TEOBResumS` at periastron, apastron, or the mean of both.

As mentioned above, time-dependent quantities like eccentricity are typically defined in terms of a reference frequency. Most eccentric models then use a reference eccentricity, e_0, that has a particular defined value at some reference frequency $f_{\rm ref}$. For `TaylorF2Ecc`, the input eccentricity and reference frequency are used to compute additional relative PN correction terms to third order. For `TEOBResumS`, e_0 and $f_{\rm ref}$ are used to determine the initial conditions that are used to evolve the trajectories of the binary components. The value of the waveform eccentricity is different than the physical, time-varying eccentricity of the system, and may also mean different things depending on the choice of model.

In this proof-of-concept study, we do not attempt to carefully standardize the definition of eccentricity between the different models used as in [46]; we merely demonstrate how well the eccentricity parameter adopted in each model can be constrained by our parameter estimation pipeline.

The waveforms described above only incorporate leading-order quadrupole radiation. During periapsis, highly eccentric compact binaries close to merger should also emit strongly in nonquadrupole modes. Some proof-of-concept studies have demonstrated how to infer parameters of generic eccentric sources including these higher-order modes, particularly in the context of numerical relativity simulations. The sources of interest in this work are low mass, long-duration sources whose strongest nonquadrupole radiation is largely at frequencies at-or-above the peak sensitivity of our detector network. As such we expect higher-order modes are relatively less important. As was done in [31], for `TEOBResumS` we include $\ell_{\rm max} \leq 4$ except the $m = 0$ modes.

C. Synthetic Population and PP tests

In this work, we use RIFT to infer the parameters of sets of populations of synthetic sources. The ranges and priors for key signal parameters are provided in Table II C. Values for each of a signal's parameters are drawn randomly from the specified range and according to the defined prior.

We focus on recovering eccentricity in the low mass regime for binary black holes. The relevant parameter ranges for our synthetic population are listed in Table II C. The individual source masses are drawn uniformly in m_i in a region bounded by $\mathcal{M}_{\rm ch}/M_\odot \in [10, 20]$ and $\eta \in [0.2, 0.25]$. The sources are placed at a luminosity distance of $500 - 1000$ Mpc, drawn proportionally to d_L^2. The eccentricity of each synthetic binary falls within $e_0 \in [0.01, 0.1]$.

For eccentric sources, we first investigate the non-spinning case and then consider aligned-spin sources, with each spin component assumed to be uniform in $[-0.5, 0.5]$. We sample over aligned-spin using an effective spin parameter

$$\chi_{\rm eff} = \frac{(m_1\chi_{1,z} + m_2\chi_{2,z})}{(m_1 + m_2)}.$$

Spin precession is not considered in this study. This is primarily due to a lack of available waveforms including both eccentricity and precession, as discussed in the previous section.

For reproducibility, we simulate signals for eccentric BBH in a three-detector network with 4096Hz

Parameter	Symbol	Prior	Injected Range
Chirp Mass	$\mathcal{M}_{\rm ch}$	uniform in m_i	$[10-20]M_\odot$
Distance	d	$\propto d_L^2$	$[500-1000]$ Mpc
Eccentricity	e_0	uniform	$[0.01, 0.1]$
Spin	$\chi_{\rm eff}$	uniform	$[-0.5, 0.5]$
Inclination	i	uniform	$[0.0, \pi]$

TABLE I. Ranges and priors for key parameters of synthetic signal set. The values for $\chi_{\rm eff}$ apply only for the aligned spin case, as $\chi_{\rm eff}$ is set to zero for the non-spinning tests.

time series in Gaussian noise with known aLIGO design PSDs. The same noise realization is used for all analysis runs. We begin the signal evolution and the likelihood integration at 20Hz. Each source has an SNR of $\sim 10-20$.

Probability-probability (PP) plots are one way to evaluate the performance of parameter inference [47]. Using RIFT on each source k with true signal parameters λ_k, we estimate the fraction of the posterior distributions which is below the true source value $\lambda_{k,\alpha}[\hat{P}_{k,\alpha}(<\lambda_{k,\alpha})]$ for each intrinsic parameter α. After reindexing the sources such that $\hat{P}_{k,\alpha}(\lambda_{k,\alpha})$ increases with k for some fixed α, a plot of k/N versus $\hat{P}_k(\lambda_{k,\alpha})$ for relevant binary parameters can be compared with the expected result $(P(<p)=p)$ and the binary uncertainty interval. Such PP plots will be shown in the results in Section IV.

III. PARAMETER DEGENERACIES

A. Chirp Mass

The authors of [14] explore a degeneracy between eccentricity and chirp mass for `TaylorF2Ecc` and introduce a new parameter called *eccentric chirp mass*. This parameter explains a bias seen in the standard chirp mass parameter when eccentricity is present in the waveform. As binary eccentricity e_0 increases, the bias in recovered chirp mass $\mathcal{M}_{\rm ch}$ grows, tending to recover a higher chirp mass than the injected value. See Figures 3 & 4 in reference [14].

The standard chirp mass for circular binaries is

$$\mathcal{M}_{\rm ch} \equiv \eta^{3/5} M_{\rm tot} = (m_1 m_2)^{3/5}(m_1+m_2)^{-1/5} \quad (1)$$

where η is the symmetric mass ratio. However, [14] defines eccentric chirp mass for low-eccentricity binaries as

$$\mathcal{M}_{\rm ch}^{\rm ecc} = \frac{\mathcal{M}_{\rm ch}}{(1-\frac{157}{24}e_0^2)^{3/5}} \quad (2)$$

which serves to replace the standard "circular" chirp mass and explain a degeneracy between eccentricity and standard $\mathcal{M}_{\rm ch}$. We find similar results using RIFT.

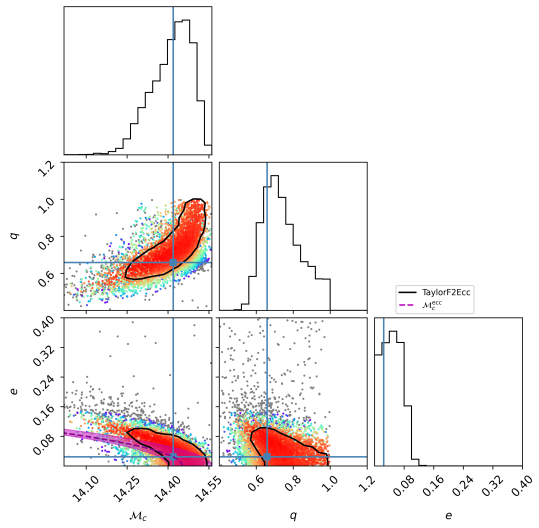

FIG. 1. A corner plot showing injection results for one synthetic signal event. The true event parameters are shown by solid blue lines. To test the eccentric chirp mass parameter, we plot the value of $\mathcal{M}_{\rm ch}^{\rm ecc}$ calculated using (2) and the true values of $\mathcal{M}_{\rm ch}$ and e_0 on the 2D recovered eccentricity-chirp mass posterior. We see that the eccentric chirp mass parameter better fits the peak of the recovered posteriors, demonstrating the expected behavior as described by [14]. Note the strong parameter correlation between eccentricity and chirp mass, shown by the recovered points and calculated by the true $\mathcal{M}_{\rm ch}^{\rm ecc}$ line.

Measurements of $\mathcal{M}_{\rm ch}$ are strongly correlated with eccentricity. We can now better constrain chirp mass using the parameter $\mathcal{M}_{\rm ch}^{\rm ecc}$ introduced in [14]. $\mathcal{M}_{\rm ch}^{\rm ecc}$ is a natural parameter that better corresponds to the shape of the $\mathcal{M}_{\rm ch}$ posterior. For this reason, we implement $\mathcal{M}_{\rm ch}^{\rm ecc}$ as an additional fitting coordinate in RIFT.

Figure 1 shows that we find the same degeneracy between eccentricity and chirp mass as discussed by [14]. In this figure we use show a fit for $\mathcal{M}_{\rm ch}^{\rm ecc}$ superimposed on our standard chirp mass posteriors after RIFT has completed parameter recovery. The points indicate individual search points in parameter spaced and are mapped to colors based on their likelihood values. Red points indicate the highest likelihoods. We plot the truth values for the injected signal as solid blue lines. The peak in the recovered posterior for chirp mass falls slightly above the injected value. When we calculate $\mathcal{M}_{\rm ch}^{\rm ecc}$ based on the true values for $\mathcal{M}_{\rm ch}$ and e_0, the magenta dashed line shows that the eccentric chirp mass more accurately finds the peak of the recovered posterior as shown in

Figure 1.

B. Argument of Periapsis

The argument of periapsis at $\omega_{\rm ref}$. This parameter is the fraction as an angle of the orbital period through which the system has rotated since the last pericenter passage. This angle is measured from the reference plane of a binary orbit to the point of periapsis passage. Eccentricity and mean anomaly are the two additional intrinsic parameters that are required to fully describe the orbit of an eccentric binary black hole system [46].

The waveform reference frequency $f_{\rm ref}$ and periapsis the reference frequency $\omega_{\rm ref}$ may not be the same when performing signal recovery. Since values of eccentricity and mean anomaly vary during binary evolution, the authors of [46] advocate for standardized definitions of a reference point at which to measure the values of these parameters, and make suggestions for how to do so.

The two waveform models used in this investigation do not allow the user to independently vary the argument of periapsis. [39] develops method to examine $\omega_{\rm ref}$ indirectly for `TEOBResumS`. The authors conclude that analyses to date are unlikely to have suffered from fixing a value for this parameter given the relatively low SNR of eccentric candidate sources. They do however recommend that future analyses marginalize over this parameter as detectors become more sensitive to potentially eccentric sources and until more waveform models become available. We also note the recent investigation [48] which performed proof-of-concept parameter inference using a new effective one-body model which implements this parameter natively.

The argument of periapsis is now availble in RIFT to be used with future waveform models that include it, in preparation to eventually test how this parameter affects parameter estimation. However, the two models used in this study do not allow direct control of this parameter so we do not use it to measure eccentricity at this time.

IV. RESULTS

In this section, we use RIFT to recover the parameters of ensembles of 100 sources whose properties were described in Section II C and which were created using the models described in Section II B.

The parameter ranges for the injected signals are shown in Table II C. We investigate both the non-spinning and aligned-spin cases for eccentric sources to demonstrate RIFT's ability to recover eccentricity well.

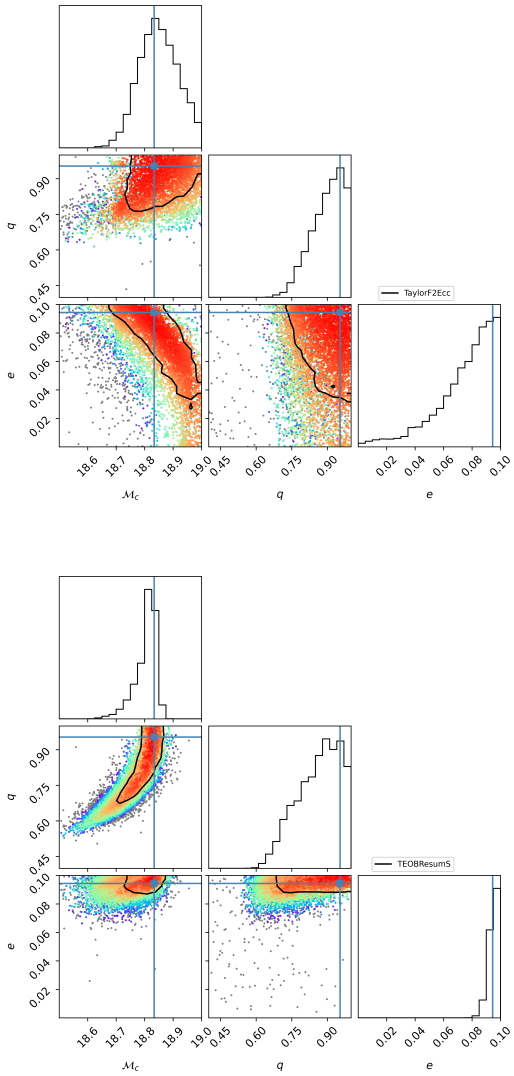

FIG. 2. Top: Corner plot showing one and two dimensional marginal distributions $\mathcal{M}_{\rm ch}, q, e$ for a signal recovered with `TaylorF2Ecc`. The injected signal has no spin. The contours represent the 90% confidence intervals for each joint distribution. Solid blue lines indicate true parameter values. This plot show $\mathcal{M}_{\rm ch}$ contours rather than $\mathcal{M}_{\rm ch}^{\rm ecc}$ contours. Bottom: corner plot showing one and two dimensional marginal distributions $\mathcal{M}_{\rm ch}, q, e$ for a signal recovered with `TEOBResumS`. The injected signal has no spin. Note that the signal parameters are identical for these two plots (besides injected and recovered waveform model).

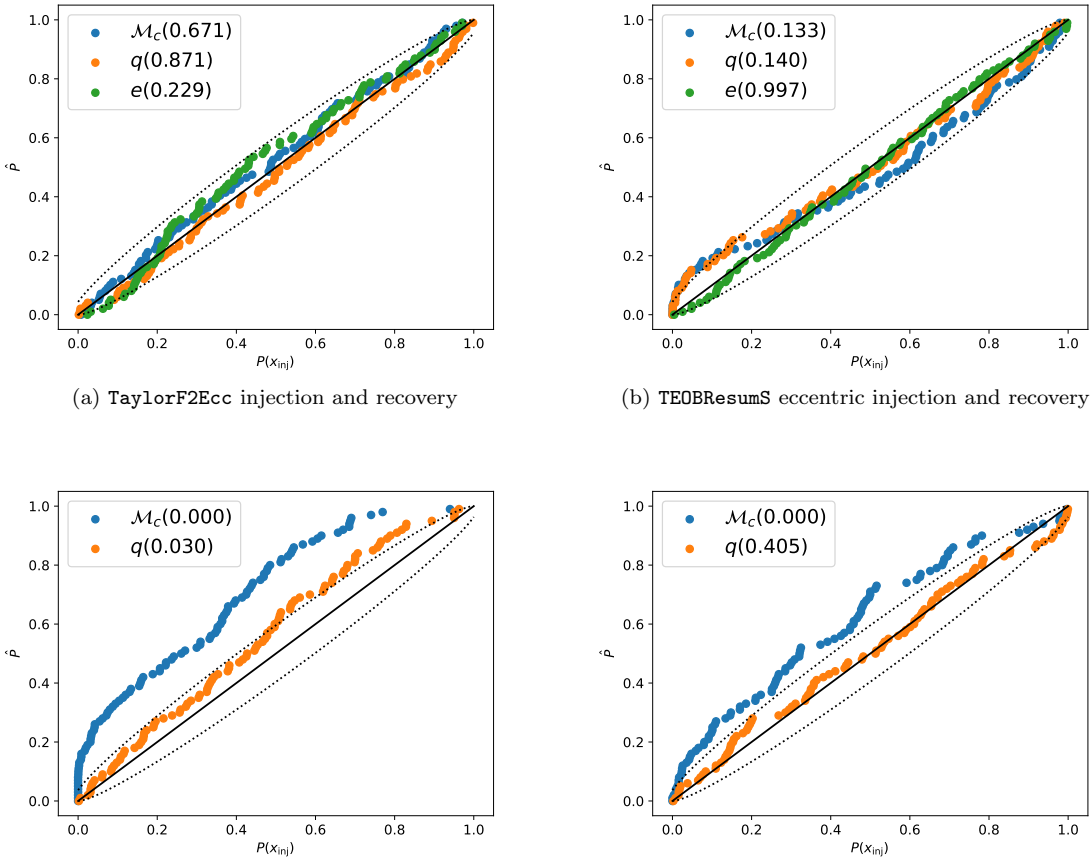

(a) `TaylorF2Ecc` injection and recovery

(b) `TEOBResumS` eccentric injection and recovery

(c) `TaylorF2` recovery of eccentric templates

(d) `TEOBResumS` eccentric injection, quasi-circular recovery templates

FIG. 3. Top-left: PP-plot of non-spinning eccentric events injected with `TaylorF2Ecc` and recovered with `TaylorF2Ecc`. Top-right: PP-plot of non-spinning eccentric events injected and then recovered with `TEOBResumS` including eccentricity. Bottom-left: Recovery of same set of non-spinning eccentric events injected with `TaylorF2Ecc`, but recovered with the quasicircular waveform model `TaylorF2`, which is equivalent to `TaylorF2Ecc` for $e = 0$. Bottom-right: Recovery of same set of non-spinning eccentric events injected with `TEOBResumS` that include eccentricity, but recovered with the non-eccentric version of `TEOBResumS`. For all plots, the dashed line indicates the 90% credible interval expected for a cumulative distribution drawn from 100 uniformly-distributed samples. All panels show recovery of the same injection set (i.e. all injection parameters are identical per event except for the waveform model), demonstrating that eccentric physics must be included in recovering eccentric waveforms regardless of waveform model.

A. Eccentric Non-spinning Recovery

We first test the ability of RIFT to recover injected signals that include eccentricity but where the binary components are non-spinning. In Figure 2, the top panel shows an example of `TaylorF2Ecc` [35] used for both injection and recovery, and the bottom panel shows an example of `TEOBResumS` [43] injection and recovery of a waveform with identical parameters as the top panel. We see that the signal is well recovered in both cases, but note definitive differences between the shapes of the posteriors depending on which waveform was used.

In this recovery set, we can use $\mathcal{M}_{\rm ch}^{\rm ecc}$ to fit the chirp mass posteriors, but we do not use this parameter for sampling. Additionally, we obtained good recovery results without the use of the argument of periapsis, which we do not use for our recovery of non-spinning eccentric signals because it is not available in the waveform implementations for either `TaylorF2Ecc` or `TEOBResumS`.

We use a PP-plot to examine whether the signal parameters are recovered well over the whole set of synthetic signals. A diagonal PP-plot indicates that

the distribution of the recovered signals matches the distribution of those injected, as described in Section II C. For our non-spinning eccentric signals, we obtain a diagonal PP-plots shown in Figure 3: our inference reliably recovers the source parameters, including eccentricity.

PP-like plots also allow us to demonstrate conclusively just how important eccentricity is when characterizing source properties. Figure 3a shows that our parameter inference is unbiased for `TaylorF2Ecc`. Then we repeat the analysis described above, but require exactly quasicircular orbits during inference: we recover eccentric non-spinning signals with a non-eccentric, non-spinning waveform. Here we use `TaylorF2`, which is the same as the `TaylorF2Ecc` model used above but excludes eccentric corrections. As seen in Figure 3c, the PP-plot is no longer diagonal: eccentric physics must be included to infer any source properties even for a population of modest-amplitude signals with observationally accessible eccentricities.

The same process is performed again using `TEOBResumS`. For this analysis we include higher order modes up to $\ell_{\rm max} = 4$ except for $m = 0$ according to the available subdominant modes for this waveform. Figure 3b shows that our parameter inference is unbiased for this second waveform as well. Then we once again repeat the analysis, but require quasicircular templates from `TEOBResumS` during inference: we recover a eccentric (non-spinning) signals made with the eccentric version of `TEOBResumS` with the non-eccentric, non-spinning version of `TEOBResumS`. As seen in Figure 3d, the PP-plot is no longer diagonal. This reiterates that eccentric physics must be included to infer any source properties — even for a population of modest-amplitude signals with observationally accessible eccentricities for both waveform models we test.

One interesting feature to note is that the strong correlation between $\mathcal{M}_{\rm ch}$ and e present in the `TaylorF2Ecc` waveform, as seen in Figure 2 and described by [14] as $\mathcal{M}_{\rm ch}^{\rm ecc}$, is missing from the `TEOBResumS` recovery, where chirp mass and eccentricity appear to be fairly uncorrelated.

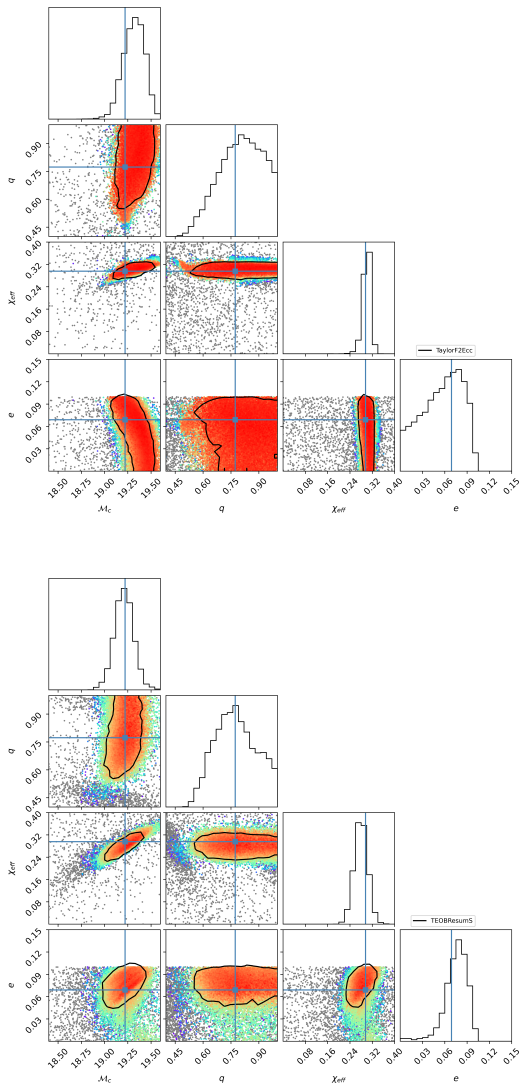

FIG. 4. Top: Corner plot showing one and two dimensional marginal distributions $\mathcal{M}_{\rm ch}, q, \chi_{\rm eff}, e$ for a signal recovered with `TaylorF2Ecc`. The injected signal has aligned spin. The contours represent the 90% confidence intervals for each joint distribution. Solid blue lines indicate true parameter values. Bottom: corner plot showing one and two dimensional marginal distributions $\mathcal{M}_{\rm ch}, q, \chi_{\rm eff}, e$ for a signal recovered with `TEOBResumS`. The injected signal has aligned spin. Note that the signal parameters are identical for these two plots (besides injected and recovered waveform model).

B. Eccentric Aligned-Spin Recovery

Similarly, we test the ability of RIFT to recover injected signals that include eccentricity where the binary components have aligned spin vectors. In Figure 4, we use `TaylorF2Ecc` [35] and `TEOBResumS` to both inject and recover these waveforms to see that the signal is well recovered.

As an anecdotal example of the importance of including eccentricity in signal recovery, we show the bias that can arise in recovered parameter values in Figure 5. We choose an example signal near the upper end of our range in eccentricity. The top corner plot shows an eccentric `TEOBResumS`signal recovered with quasi-circular waveform template. In this ex-

ample, we attempt to recover the parameter values of an eccentric signal without considering eccentricity. We see that the recovery completely misses the value of the chirp mass. However, when we do consider eccentricity in the recovery of this same eccentric signal, as shown in the bottom corner plot of Figure 5, the values of the parameters are much more accurately recovers. This illustrates the importance of the inclusion of eccentricity in the recovery of eccentric signals.

We use a PP-plot to examine whether the signal parameters are recovered well over the whole set of synthetic signals. A diagonal PP-plot indicates that the distribution of the recovered signals matches the distribution of those injected, as described in Section II C. For our aligned-spin eccentric signals, we obtain a diagonal PP-plots shown in Figure 6; our inference reliably recovers the source parameters, including eccentricity and aligned-spin.

To perform the aligned-spin analysis, we use the Rotated Inspiral-Phase (RIP) coordinates added in [38] in the CIP step of our parameter recovery. These coordinates are particularly useful in the low-mass regime.

PP-like plots also allow us to demonstrate conclusively just how important eccentricity is when characterizing source properties. Figure 6a shows that our parameter inference is unbiased for `TaylorF2Ecc`. Then we repeat the analysis described above, but require exactly quasicircular orbits during inference: we recover eccentric non-spinning signals with a non-eccentric, non-spinning waveform. Here we use `TaylorF2`, which is the same as the `TaylorF2Ecc` model used above but excludes eccentric corrections.

The same process is performed again using `TEOBResumS`. For this analysis we include higher order modes up to $\ell_{\rm max} = 4$ except for $m = 0$ according to the available subdominant modes for this waveform. Figure 6b shows that our parameter inference is unbiased for this second waveform as well. Then we once again repeat the analysis, but require quasicircular templates from `TEOBResumS` during inference: we recover a eccentric (non-spinning) signals made with the eccentric version of `TEOBResumS` with the non-eccentric, non-spinning version of `TEOBResumS`.

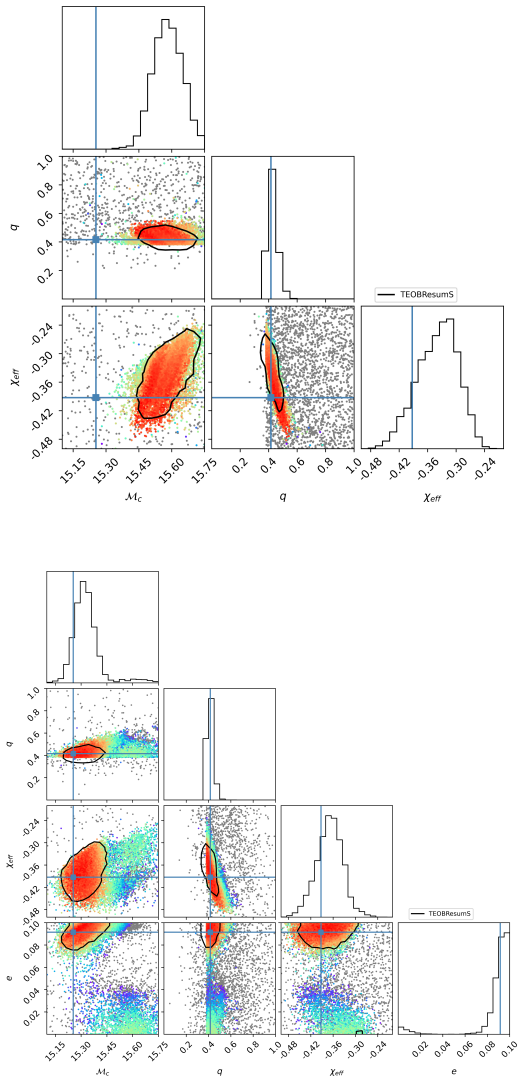

FIG. 5. Top: Corner plot showing one and two dimensional marginal distributions $\mathcal{M}_{\rm ch}, q, \chi_{\rm eff}$ for an eccentric signal recovered with a quasi-circular `TEOBResumS` template. The injected signal has aligned spin. Note the poor recovery of $\mathcal{M}_{\rm ch}$ when eccentricity is not considered in signal recovery. Bottom: corner plot showing one and two dimensional marginal distributions $\mathcal{M}_{\rm ch}, q, \chi_{\rm eff}, e$ for *the same* eccentric signal recovered with an *eccentric* `TEOBResumS` template. The accuracy of the recovered signal parameters drastically improves when eccentric recovery methods are used.

V. CONCLUSIONS

We have demonstrated that RIFT can recover eccentricity in both the non-spinning and aligned-spin cases using `TaylorF2Ecc` and `TEOBResumS` for low-mass binary black holes. This study illustrates that it is crucial to include eccentricity in parameter estimation for eccentric binary systems, otherwise recovery of source parameters will be skewed. Conversely, corroborating prior investigations, our study demonstrates that in low mass binaries the eccentricity can be measured with exquisite precision, owing to the large number of cycles available in these sys-

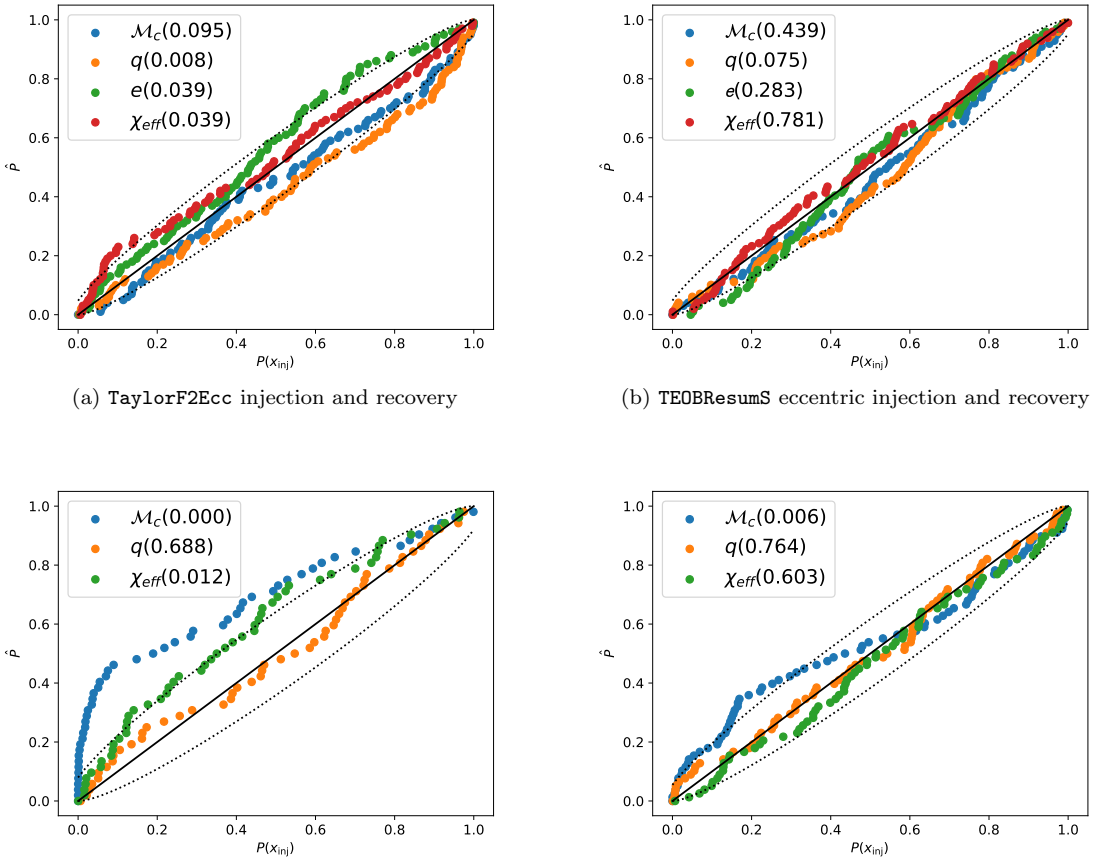

(a) `TaylorF2Ecc` injection and recovery

(b) `TEOBResumS` eccentric injection and recovery

(c) `TaylorF2` recovery of `TaylorF2Ecc` templates

(d) `TEOBResumS` quasi-circular recovery of eccentric injections

FIG. 6. Top-left: PP-plot of aligned-spin eccentric events injected with `TaylorF2Ecc` and recovered with `TaylorF2Ecc`. Top-right: PP-plot of aligned-spin eccentric events injected and then recovered with `TEOBResumS` including eccentricity. Bottom-left: Recovery of same set of aligned-spin eccentric events injected with `TaylorF2Ecc`, but recovered with the quasicircular waveform model `TaylorF2`, which is equivalent to `TaylorF2Ecc` for $e = 0$. Bottom-right: Recovery of same set of aligned-spin eccentric events injected with `TEOBResumS` that include eccentricity, but recovered with the non-eccentric version of `TEOBResumS`. For all plots, the dashed line indicates the 90% credible interval expected for a cumulative distribution drawn from 100 uniformly-distributed samples. All panels show recovery of the same injection set (i.e. all injection parameters are identical per event except for the waveform model), demonstrating that eccentric physics must be included in recovering eccentric waveforms regardless of waveform model.

tems. Finally, we introduce a new parameter to the RIFT pipeline to prepare for future parameter estimation systematics as we await new discoveries in LIGO O4. This work also prepares the pipeline to perform systematics studies for systems that include both eccentricity and spin-precession as additional waveform models become available.

As noted in prior work, our study also demonstrates how waveform systematics can impact the recovery of parameters like eccentricity; see, e.g., our Figure 4 for an example. Evidently, precise measurements of eccentricity in low-mass binary black holes may require further improvements in waveform models. That said, in our study, contemprary models seem to clearly unambiguously indicate the impact of eccentricity, such that the presence of measurable eccentricity is more robustly characterized than its precise value. Given the astrophysical implications of the unambiguous identification of eccentricity in a compact binary inspiral waveform, our investigation suggests that parameter inferences with contemporary models provide a constructive avenue to identify eccentricity in low-mass binaries.

ACKNOWLEDGMENTS

ROS and KJW gratefully acknowledge support from NSF award PHY-2012057. ROS is acknowledges support from NSF PHY-2309172 and PHY-2207920. The authors are grateful for computational resources provided by the LIGO Laboratories at CIT, LHO, and LLO supported by National Science Foundation Grants PHY-0757058 and PHY-0823459 which are used for the parameter estimation runs. This material is based upon work supported by NSF's LIGO Laboratory which is a major facility fully funded by the National Science Foundation.

[1] B. Abbott et al. (The LIGO Scientific Collaboration), Advanced LIGO, Class. Quant. Grav. **32**, 074001 (2015), arXiv:1411.4547 [gr-qc].

[2] F. e. a. Acernese, Advanced Virgo: a second-generation interferometric gravitational wave detector, Class. Quant. Grav. **32**, 024001 (2015), arXiv:1408.3978 [gr-qc].

[3] R. e. a. Abbott, The LIGO Scientific Collaboration, The Virgo Collaboration, and The KAGRA Collaboration, GWTC-3: Compact binary coalescences observed by ligo and virgo during the second part of the third observing run (2021).

[4] P. C. Peters, Gravitational radiation and the motion of two point masses, Phys. Rev. **136**, B1224 (1964).

[5] M. Zevin, C. Pankow, C. L. Rodriguez, L. Sampson, E. Chase, V. Kalogera, and F. A. Rasio, Constraining Formation Models of Binary Black Holes with Gravitational-wave Observations, Astrophysical Journal **846**, 82 (2017), arXiv:1704.07379 [astro-ph.HE].

[6] C. L. Rodriguez, P. Amaro-Seoane, S. Chatterjee, K. Kremer, F. A. Rasio, J. Samsing, C. S. Ye, and M. Zevin, Post-newtonian dynamics in dense star clusters: Formation, masses, and merger rates of highly-eccentric black hole binaries, Phys. Rev. D **98**, 123005 (2018).

[7] J. Samsing, Eccentric black hole mergers forming in globular clusters, Phys. Rev. D **97**, 103014 (2018).

[8] I. Mandel and A. Farmer, Merging stellar-mass binary black holes, Physics Reports **955**, 1 (2022).

[9] I. Mandel and R. O'Shaughnessy, Compact binary coalescences in the band of ground-based gravitational-wave detectors, Classical and Quantum Gravity **27**, 114007 (2010).

[10] C. L. Rodriguez, P. Amaro-Seoane, S. Chatterjee, and F. A. Rasio, Post-newtonian dynamics in dense star clusters: Highly eccentric, highly spinning, and repeated binary black hole mergers, Phys. Rev. Lett. **120**, 151101 (2018).

[11] J. Samsing, M. MacLeod, and E. Ramirez-Ruiz, The formation of eccentric compact binary inspirals and the role of gravitational wave emission in binary–single stellar encounters, The Astrophysical Journal **784**, 71 (2014).

[12] M. Zevin, J. Samsing, C. Rodriguez, C.-J. Haster, and E. Ramirez-Ruiz, Eccentric black hole mergers in dense star clusters: The role of binary–binary encounters, Astrophysical Journal **871**, 10.3847/1538-4357/aaf6ec (2019).

[13] M. Zevin, I. M. Romero-Shaw, K. Kremer, E. Thrane, and P. D. Lasky, Implications of eccentric observations on binary black hole formation channels, The Astrophysical Journal Letters **921**, L43 (2021).

[14] M. Favata, C. Kim, K. Arun, J. Kim, and H. W. Lee, Constraining the orbital eccentricity of inspiralling compact binary systems with advanced LIGO, Phys. Rev. D **105**, 10.1103/physrevd.105.023003 (2022).

[15] M. E. Lower, E. Thrane, P. D. Lasky, and R. Smith, Measuring eccentricity in binary black hole inspirals with gravitational waves, Physical Review D **98**, 10.1103/physrevd.98.083028 (2018).

[16] P. Saini, Resolving the eccentricity of stellar mass binary black holes with next generation ground-based gravitational wave detectors, Monthly Notices of the Royal Astronomical Society **528**, 833–842 (2024).

[17] J. Aasi et al (The LIGO Scientific Collaboration and the Virgo Collaboration), Parameter estimation for compact binary coalescence signals with the first generation gravitational-wave detector network, Phys. Rev. D **88**, 062001 (2013).

[18] I. M. Romero-Shaw, P. D. Lasky, and E. Thrane, Searching for eccentricity: signatures of dynamical formation in the first gravitational-wave transient catalogue of ligo and virgo, Monthly Notices of the Royal Astronomical Society **490**, 5210–5216 (2019).

[19] B. Abbott et al. (The LIGO Scientific Collaboration), Search for eccentric binary black hole mergers with Advanced LIGO and Advanced Virgo during their first and second observing runs, The Astrophysical Journal **883**, 149 (2019).

[20] Q.-Y. Yun, W.-B. Han, G. Wang, and S.-C. Yang, Investigating eccentricities of the binary black hole signals from the ligo-virgo catalog gwtc-1 (2020), arXiv:2002.08682 [gr-qc].

[21] S. Wu, Z. Cao, and Z.-H. Zhu, Measuring the eccentricity of binary black holes in gwtc-1 by using the inspiral-only waveform, Monthly Notices of the Royal Astronomical Society **495**, 466–478 (2020).

[22] A. Bonino, R. Gamba, P. Schmidt, A. Nagar, G. Pratten, M. Breschi, P. Rettegno, and S. Bernuzzi, Inferring eccentricity evolution from observations of coalescing binary black holes, Physical Review D **107**, 10.1103/physrevd.107.064024 (2023).

[23] E. O'Shea and P. Kumar, Correlations in gravitational-wave reconstructions from eccentric binaries: A case study with gw151226 and

gw170608, Physical Review D **108**, 10.1103/physrevd.108.104018 (2023).
[24] I. Romero-Shaw, P. D. Lasky, E. Thrane, and J. C. Bustillo, Gw190521: Orbital eccentricity and signatures of dynamical formation in a binary black hole merger signal, The Astrophysical Journal Letters **903**, L5 (2020).
[25] V. Gayathri, J. Healy, J. Lange, B. O'Brien, M. Szczepanczyk, I. Bartos, M. Campanelli, S. Klimenko, C. Lousto, and R. O'Shaughnessy, Eccentricity estimate for black hole mergers with numerical relativity simulations (2022), arXiv:2009.05461 [astro-ph.HE].
[26] R. Gamba, M. Breschi, G. Carullo, P. Rettegno, S. Albanesi, S. Bernuzzi, and A. Nagar, Gw190521 as a dynamical capture of two nonspinning black holes (2022), arXiv:2106.05575 [gr-qc].
[27] I. M. Romero-Shaw, N. Farrow, S. Stevenson, E. Thrane, and X.-J. Zhu, On the origin of gw190425, Monthly Notices of the Royal Astronomical Society: Letters **496**, L64–L69 (2020).
[28] A. K. Lenon, A. H. Nitz, and D. A. Brown, Measuring the eccentricity of gw170817 and gw190425, Monthly Notices of the Royal Astronomical Society **497**, 1966–1971 (2020).
[29] I. Romero-Shaw, P. D. Lasky, and E. Thrane, Signs of eccentricity in two gravitational-wave signals may indicate a subpopulation of dynamically assembled binary black holes, Astrophysical Journal **921**, L31 (2021).
[30] I. Romero-Shaw, P. D. Lasky, and E. Thrane, Four eccentric mergers increase the evidence that ligo–virgo–kagra's binary black holes form dynamically, The Astrophysical Journal **940**, 171 (2022).
[31] H. L. Iglesias, J. Lange, I. Bartos, S. Bhaumik, R. Gamba, V. Gayathri, A. Jan, R. Nowicki, R. O'Shaughnessy, D. Shoemaker, R. Venkataramanan, and K. Wagner, Eccentricity estimation for five binary black hole mergers with higher-order gravitational wave modes (2023), arXiv:2208.01766 [gr-qc].
[32] T. LIGO Scientific Collaboration, the Virgo Collaboration, and the KAGRA Collaboration: A. G. Abac et al., Search for eccentric black hole coalescences during the third observing run of LIGO and Virgo (2023), arXiv:2308.03822 [astro-ph.HE].
[33] A. Nagar, A. Bonino, and P. Rettegno, Effective one-body multipolar waveform model for spin-aligned, quasicircular, eccentric, hyperbolic black hole binaries, Phys. Rev. D **103**, 104021 (2021), arXiv:2101.08624 [gr-qc].
[34] Z. Cao and W.-B. Han, Waveform model for an eccentric binary black hole based on the effective-one-body-numerical-relativity formalism, Phys. Rev. D **96**, 044028 (2017).
[35] B. Moore, M. Favata, K. Arun, and C. K. Mishra, Gravitational-wave phasing for low-eccentricity inspiralling compact binaries to 3pn order, Phys. Rev. D **93**, 10.1103/physrevd.93.124061 (2016).
[36] Divyajyoti, S. Kumar, S. Tibrewal, I. M. Romero-Shaw, and C. K. Mishra, Blind spots and biases: the dangers of ignoring eccentricity in gravitational-wave signals from binary black holes (2023), arXiv:2309.16638 [gr-qc].
[37] J. Lange, R. O'Shaughnessy, and M. Rizzo, Rapid and accurate parameter inference for coalescing, precessing compact binaries, arXiv e-prints , arXiv:1805.10457 (2018), arXiv:1805.10457 [gr-qc].
[38] J. Wofford, A. B. Yelikar, H. Gallagher, E. Champion, D. Wysocki, V. Delfavero, J. Lange, C. Rose, V. Valsan, S. Morisaki, J. Read, C. Henshaw, and R. O'Shaughnessy, Improving performance for gravitational-wave parameter inference with an efficient and highly-parallelized algorithm, Phys. Rev. D **107**, 024040 (2023).
[39] T. A. Clarke, I. M. Romero-Shaw, P. D. Lasky, and E. Thrane, Gravitational-wave inference for eccentric binaries: the argument of periapsis, Monthly Notices of the Royal Astronomical Society **517**, 3778 (2022).
[40] T. Damour and G. Schaefer, Higher Order Relativistic Periastron Advances and Binary Pulsars, Nuovo Cim. B **101**, 127 (1988).
[41] G. Schäfer and N. Wex, Second post-newtonian motion of compact binaries, Physics Letters A **177**, 461 (1993).
[42] LIGO Scientific Collaboration, LIGO Algorithm Library - LALSuite, free software (GPL) (2018).
[43] A. Nagar, S. Bernuzzi, W. D. Pozzo, G. Riemenschneider, S. Akcay, G. Carullo, P. Fleig, S. Babak, K. W. Tsang, M. Colleoni, F. Messina, G. Pratten, D. Radice, P. Rettegno, M. Agathos, E. Fauchon-Jones, M. Hannam, S. Husa, T. Dietrich, P. Cerdá-Duran, J. A. Font, F. Pannarale, P. Schmidt, and T. Damour, Time-domain effective-one-body gravitational waveforms for coalescing compact binaries with nonprecessing spins, tides, and self-spin effects, Phys. Rev. D **98**, 10.1103/physrevd.98.104052 (2018).
[44] A. Buonanno and T. Damour, Effective one-body approach to general relativistic two-body dynamics, Phys. Rev. D **59**, 10.1103/physrevd.59.084006 (1999).
[45] D. Chiaramello and A. Nagar, Faithful analytical effective-one-body waveform model for spin-aligned, moderately eccentric, coalescing black hole binaries, Phys. Rev. D **101**, 101501 (2020), arXiv:2001.11736 [gr-qc].
[46] M. A. Shaikh, V. Varma, H. P. Pfeiffer, A. Ramos-Buades, and M. van de Meent, Defining eccentricity for gravitational wave astronomy (2023), arXiv:2302.11257 [gr-qc].
[47] S. R. Cook, A. Gelman, and D. B. Rubin, Validation of software for bayesian models using posterior quantiles, Journal of Computational and Graphical Statistics **15**, 675 (2006).
[48] A. Ramos-Buades, A. Buonanno, and J. Gair, Bayesian inference of binary black holes with inspiral-merger-ringdown waveforms using two eccentric parameters (2023), arXiv:2309.15528 [gr-qc].